Journal of Computational and Applied Mathematics 233 (2010) 3095–3102

Contents lists available at ScienceDirect

Journal of Computational and Applied Mathematics

journal homepage: www.elsevier.com/locate/cam

Finite element LES and VMS methods on tetrahedral meshes

Volker John *, Adela Kindl, Carina Suciu

FR 6.1 – Mathematik, Universität des Saarlandes, Postfach 15 11 50, 66041 Saarbrücken, Germany

ARTICLE INFO

Article history:
Received 30 March 2009

Keywords:
Incompressible Navier–Stokes equations
Turbulent flows
Large Eddy Simulation
Variational multiscale methods
Tetrahedral meshes

ABSTRACT

Finite element methods for problems given in complex domains are often based on tetrahedral meshes. This paper demonstrates that the so-called rational Large Eddy Simulation model and a projection-based Variational Multiscale method can be extended in a straightforward way to tetrahedral meshes. Numerical studies are performed with an inf–sup stable second order pair of finite elements with discontinuous pressure approximation.

1. Introduction

The accurate simulation of turbulent incompressible flows is a major challenge, as not all scales appearing in a turbulent flow can be simulated. Popular methods for simulating turbulent flows include Large Eddy Simulation (LES) [1], which decomposes the flow field into large (resolved) scales and small (unresolved) scales and aims at an accurate simulation of only the large scales. Variational multiscale (VMS) methods are a rather new alternative to the classical LES, based on ideas from [2,3], with first applications to turbulent flow simulations in [4]. An essential difference to classical LES is the definition of scales by projections into appropriate function spaces, rather than the classical spatial averaging (filtering).

The simplest and (for this reason) most popular LES method is the Smagorinsky LES model [1,5]. It adds a nonlinear eddy viscosity model to the momentum equation. This model contains a parameter which is chosen in practice, either as a constant (static Smagorinsky model) or a posteriorly as a function of space and time (dynamic Smagorinsky model, [6,7]).

A main issue in LES is the modeling of the so-called Reynolds stress tensor in terms of the large scales defined by spatial filtering. Using the Gaussian filter, the key of deriving a model consists in approximating the Fourier transform of this filter with a simpler function. An early proposal from [8] used a second order Taylor polynomial. However, it turned out that this model does not damp the high wave number components appropriately. Based on this observation, in [9], it was proposed to use a second order rational approximation. The resulting LES model is called rational LES model. Details of its derivation can be found in [9–11]. Numerical studies [10,12] show that this model alone does not suffice for stable simulations of turbulent flows. Another model for the so-called subgrid scale tensor is needed. For this purpose, the static Smagorinsky model is often used; see the simulations in [10–12].

There are drawbacks in the way LES defines the large scales. The assumed commutation of spatial filtering and spatial differentiation does not hold in bounded domains (as often given in applications) or for non-constant filter widths. A mathematical analysis of the resulting commutation errors shows that they are non-negligible in the vicinity of the domain's boundary [10,13–15]. In addition, correct boundary conditions for the spatially averaged large scales are not known; see [9,10,16] for explanations and proposals. The definition of large scales by variational projections, in the way it is done in VMS methods, avoids these difficulties.

* Corresponding author. Tel.: +49 681 302 2784; fax: +49 681 302 4443.
E-mail addresses: john@math.uni-sb.de (V. John), adela@c-kindl.de (A. Kindl), suciu@math.uni-sb.de (C. Suciu).

0377-0427/$ – see front matter © 2009 Elsevier B.V. All rights reserved.
doi:10.1016/j.cam.2009.06.005

For an introduction as well as a review to VMS methods we refer to [4,17,18]. Meanwhile, there exist several realizations of VMS methods, [19–21], and the available proposals are quite different. We will concentrate here on finite element VMS (FEVMS) methods. See the review in [19] for VMS methods based on other discretizations.

This paper considers a VMS method which relies on a three-scale decomposition of the flow field into large, resolved small and unresolved (small) scales [22]. Assuming that the direct influence of the unresolved scales onto the large scales can be neglected, the influence of the unresolved small scales is described by a model which acts directly only on the resolved small scales rather than on all resolved scales, which is the case in the classical LES. The parameters of this so-called projection-based FEVMS method are the turbulence model acting directly on the resolved small scales, and the finite element spaces defining the scale separation. Almost all numerical simulations with VMS methods use eddy viscosity models of Smagorinsky-type, for instance [19,22–27]. Such a model will be considered also here. Regarding the spaces for the scale separation, the projection-based three-scale FEVMS method uses standard finite element spaces for all resolved scales. The separation of the large scales and the resolved small scales is achieved via an additional space for the large scales. The projection for the definition of the scales is given explicitly as an additional equation.

Numerical studies with the projection-based FEVMS method [19,21,26] have shown that the choice of the large scale space has a high impact on the results. This space controls the effect of the turbulence model. In these studies, the additional large scale space has been chosen a priorly, being the same for all mesh cells, and remained unchanged during the whole simulation. It could be observed that the influence of the actual form of the turbulence model on the results was considerably smaller than the influence of the large scale space. Considering this, and the fact that in a turbulent flow not every region of the flow domain presents the same amount of turbulence, in [20] an extension of the projection-based FEVMS method was presented, where the large scale space was computed a posteriorly and adaptively, allowing different local large scale spaces in different mesh cells. This way, the effect of the turbulence model was controlled by an appropriate local choice of the large scale space.

The goal of this paper consists in demonstrating that the rational LES method and the projection-based FEVMS method can be extended straightforwardly to discretizations on tetrahedral grids. This fact seems to us to be important since the complexity of the domains in applications often does not allow the use of hexahedral meshes. In addition, there are many more mesh generators for tetrahedral meshes available than for hexahedral meshes. On the other hand, standard benchmark problems for turbulent flow simulations, like decaying isotropic turbulence or turbulent channel flows, are defined on rather simple domains, such that the vast majority of simulations which can be found in the literature uses discretizations which are well suited for such domains, like finite difference methods or spectral methods.

An important observation for a multitude of simulations of incompressible flows on hexahedral grids was that an inf–sup stable pair of finite elements with second order velocity and first order, discontinuous pressure (Q_2/P_1^{disc}) performed best with respect to the ratio of accuracy and efficiency [28,29]. The straightforward extension of this pair to tetrahedra does not satisfy the inf–sup condition. An enrichment of the velocity space with bubble functions (cell and face bubbles) becomes necessary [30], leading to the $P_2^{\text{bubble}}/P_1^{\text{disc}}$ pair of finite element spaces, which will be used in the simulations presented in this paper. In addition, the use of a velocity finite element of at least second order is important for the application of the projection-based FEVMS [22]. To our best knowledge, numerical studies of incompressible turbulent flows in three dimensions using this pair of finite elements are not yet available.

The paper is organized as follows. Section 2 presents the turbulence models. Details of the discretizations are provided at the beginning of Section 3. This section contains also the numerical studies. Section 4 gives a summary of the results.

2. The turbulence models

2.1. The incompressible Navier–Stokes equations

Incompressible flows are governed by the incompressible Navier–Stokes equations. We consider a space-time domain $\Omega \times [0, T] \subset \mathbb{R}^3 \times \mathbb{R}_0^+$, where Ω is bounded, connected, with polyhedral boundary $\partial\Omega$. The problem consists of solving the following equations for $\mathbf{u}$, the fluid velocity and p, the pressure:

$$\begin{aligned} &\mathbf{u}_t - 2\nu\nabla\cdot\mathbb{D}(\mathbf{u}) + (\mathbf{u}\cdot\nabla)\mathbf{u} + \nabla p = \mathbf{f} && \text{in } \Omega \times (0, T], \\ &\nabla\cdot\mathbf{u} = 0 && \text{in } \Omega \times [0, T], \\ &\mathbf{u}(0, \mathbf{x}) = \mathbf{u}_0 && \text{in } \Omega, \end{aligned} \tag{1}$$

with $\mathbf{f}$ being an external force, ν the kinematic viscosity, assumed positive and constant, $\mathbf{u}_0$ the initial velocity field, $\mathbb{D}(\mathbf{u}) = (\nabla\mathbf{u} + (\nabla\mathbf{u})^{\mathrm{T}})/2$ the velocity deformation tensor (symmetric part of the gradient). The equations (1) have to be closed with appropriate boundary conditions.

There is no exact definition of what a turbulent flow is. From the mathematical point of view, turbulent flows occur for large Reynolds numbers $Re = \mathcal{O}(\nu^{-1})$. From the physical point of view, turbulent flows are characterized by a richness of scales (flow structures), ranging from very large ones to very small ones. Present days simulation capacities allow discretizations (grids) which can represent only the largest scales. This is a fundamental difficulty of turbulent flow simulations since the small scales, which cannot be resolved and consequently not be simulated, are important for the turbulent character of the flow [31]. Turbulence modeling aims to model the influence of the unresolved scales onto the resolved large scales.

2.2. The Smagorinsky LES model

Let $\Omega = \mathbb{R}^3$. LES starts by defining large scales $(\overline{\mathbf{u}}, \overline{p})$ by spatial averaging

$$\overline{\mathbf{u}}(\mathbf{y}) = \frac{1}{\delta(\mathbf{y})^d} \int_{\mathbb{R}^d} g\left(\frac{\mathbf{y}-\mathbf{x}}{\delta(\mathbf{y})}\right) \mathbf{u}(\mathbf{x})\, d\mathbf{x}, \qquad \overline{p}(\mathbf{y}) = \frac{1}{\delta(\mathbf{y})^d} \int_{\mathbb{R}^d} g\left(\frac{\mathbf{y}-\mathbf{x}}{\delta(\mathbf{y})}\right) p(\mathbf{x})\, d\mathbf{x}.$$

The parameter $\delta(\mathbf{y})$ is the so-called filter width and $g(\cdot)$ is the filter function. The small scales or fluctuations are defined by $\mathbf{u}' = \mathbf{u} - \overline{\mathbf{u}}, \quad p' = p - \overline{p}$. The derivation of equations for the large scales starts by filtering the Navier–Stokes equations (1). Assuming that filtering and differentiation commute, one ends up with the space averaged Navier–Stokes equations

$$\begin{aligned} &\frac{\partial \overline{\mathbf{u}}}{\partial t} - 2Re^{-1}\nabla\cdot\mathbb{D}(\overline{\mathbf{u}}) + \nabla\cdot(\overline{\mathbf{u}}\,\overline{\mathbf{u}}^{\mathrm{T}}) + \nabla\cdot\mathcal{R}(\mathbf{u},\mathbf{u}) + \nabla\overline{p} = \overline{\mathbf{f}} && \text{in } \mathbb{R}^d\times(0,T],\\ &\nabla\cdot\overline{\mathbf{u}} = 0 && \text{in } \mathbb{R}^d\times(0,T],\\ &\overline{\mathbf{u}}(0,\cdot) = \overline{\mathbf{u}_0} && \text{in } \mathbb{R}^d, \end{aligned} \tag{2}$$

with the Reynolds stress tensor

$$\mathcal{R}(\mathbf{u},\mathbf{u}) = \overline{\mathbf{u}\mathbf{u}^{\mathrm{T}}} - \overline{\mathbf{u}}\,\overline{\mathbf{u}}^{\mathrm{T}} = \overline{\overline{\mathbf{u}}\,\overline{\mathbf{u}}^{\mathrm{T}}} + \overline{\overline{\mathbf{u}}\,\mathbf{u}'^{\mathrm{T}}} + \overline{\mathbf{u}'\overline{\mathbf{u}}^{\mathrm{T}}} + \overline{\mathbf{u}'\mathbf{u}'^{\mathrm{T}}} - \overline{\mathbf{u}}\,\overline{\mathbf{u}}^{\mathrm{T}}. \tag{3}$$

As already mentioned in the introduction, the commutation assumption is in general not valid, in particular if Ω is a bounded domain [10,13–15]. For bounded domains, the usual way in LES practice consists in restricting (2) to Ω. The main issue in LES consists in modeling the Reynolds stress tensor (3) in terms of the large scales.

The simplest model is the Smagorinsky model which is based on physical insight and similarity assumptions [5,31,1]. The momentum equation of the Smagorinsky LES model has the form

$$\mathbf{u}_t - \nabla\cdot\left(\left(2\nu + C_S\delta^2\,\|\mathbb{D}(\mathbf{u})\|_F\right)\mathbb{D}(\mathbf{u})\right) + (\mathbf{u}\cdot\nabla)\mathbf{u} + \nabla p = \mathbf{f} \quad \text{in } \Omega\times(0,T] \tag{4}$$

where C_S is a parameter and $\|\cdot\|_F$ the Frobenius norm of a tensor. If $C_S > 0$ is chosen to be a constant, (4) is called the static Smagorinsky model. A good choice of C_S is in general difficult. In fact, the static Smagorinsky model turns out to be in general too diffusive. There is a so-called dynamic Smagorinsky model [6,7] which computes C_S a posteriorly in space and time. However, recent studies show that the parameters obtained in this way can much differ from optimal parameters [32].

The Smagorinsky LES model possesses more favorable analytical properties than the Navier–Stokes equations. For instance, the existence and uniqueness of a weak solution can be shown [33,34] and finite element estimates can be found in [35].

2.3. The rational LES model

The derivation of the rational LES model starts by considering the Fourier transform of the individual terms of the Reynolds stress tensor (3), where the filter function is the Gaussian filter

$$g_\delta(\mathbf{x}) = \left(\frac{6}{\delta^2\pi}\right)^{d/2} \exp\left(-\frac{6}{\delta^2}\,\|\mathbf{x}\|_2^2\right)$$

with the constant filter width $\delta > 0$. Approximating the Fourier transform of this filter with a rational function (second order Padé approximation), one gets after applying the inverse Fourier transform and neglecting terms of higher order [9–11,29]

$$\mathcal{R}(\mathbf{u},\mathbf{u}) \approx \frac{\delta^2}{2\gamma}\left(I - \frac{\delta^2}{4\gamma}\Delta\right)^{-1} \nabla\overline{\mathbf{u}}\,\nabla\overline{\mathbf{u}}^{\mathrm{T}}.$$

In this derivation, the subgrid scale term $\overline{\mathbf{u}'\mathbf{u}'^{\mathrm{T}}}$ contributes only to the higher order terms and it is consequently modeled by zero. Numerical studies have shown that this model is not sufficient [12]. There are several proposals for appropriate models of $\overline{\mathbf{u}'\mathbf{u}'^{\mathrm{T}}}$ [10,11]. We will use here the static Smagorinsky model such that the momentum equation of the rational LES model becomes

$$\begin{aligned} &\mathbf{u}_t - \nabla\cdot\left(\left(2\nu + C_S\delta^2\,\|\mathbb{D}(\overline{\mathbf{u}})\|_F\right)\mathbb{D}(\mathbf{u})\right) + (\mathbf{u}\cdot\nabla)\mathbf{u} + \nabla p + \nabla\cdot\left(\frac{\delta^2}{2\gamma}\left(I - \frac{\delta^2}{4\gamma}\Delta\right)^{-1}\nabla\overline{\mathbf{u}}\,\nabla\overline{\mathbf{u}}^{\mathrm{T}}\right) = \mathbf{f}\\ &\text{in } \Omega\times(0,T]. \end{aligned} \tag{5}$$

2.4. The projection-based FEVMS method

VMS methods are an approach to control the influence of the turbulence model in an appropriate way. This is done by choosing resolved scales which are directly influenced by this model. The projection-based FEVMS method uses standard

finite element spaces to model all resolved scales, and an additional space is introduced in order to decompose the resolved scales into large and small ones. The large scales are defined by a variational projection into this large scale space, the projection being given explicitly as an additional equation. Together with the unresolved scales, a three-scale decomposition of the flow field is achieved. The decomposition of the resolved scales will control the direct influence of the turbulence model.

VMS methods are based on a variational formulation of the underlying equation. Let $V^h \times Q^h$ be the pair of inf–sup stable, conforming finite element spaces for the velocity and pressure. Consider the additional large scale space as being the finite dimensional space of symmetric $d \times d$ tensor-valued functions $L^H \subset \{\mathbb{L} \in (L^2(\Omega))^{d\times d}, \mathbb{L}^{\mathrm{T}} = \mathbb{L}\}$. Let ν_T be a non-negative function representing the turbulent viscosity. The semi-discrete (continuous in time) projection-based FEVMS method then seeks $\mathbf{u}^h : [0,\ T] \to V^h, p^h : (0,\ T] \to Q^h$, and $\mathbb{G}^H : [0,\ T] \to L^H$ such that

$$\begin{aligned}
&(\mathbf{u}_t^h,\ \mathbf{v}^h) + (2\nu\mathbb{D}(\mathbf{u}^h),\ \mathbb{D}(\mathbf{v}^h)) + ((\mathbf{u}^h\cdot\nabla)\mathbf{u}^h,\ \mathbf{v}^h) - (p^h,\ \nabla\cdot\mathbf{v}^h) + (\nu_T(\mathbb{D}(\mathbf{u}^h) - \mathbb{G}^H), \mathbb{D}(\mathbf{v}^h)) = (\mathbf{f},\ \mathbf{v}^h), \quad \forall \mathbf{v}^h \in V^h,\\
&(q^h,\ \nabla\cdot\mathbf{u}^h) = 0, \quad \forall q^h \in Q^h,\\
&(\mathbb{D}(\mathbf{u}^h) - \mathbb{G}^H,\ \mathbb{L}^H) = 0, \quad \forall \mathbb{L}^H \in L^H.
\end{aligned} \tag{6}$$

The large scales of $\mathbb{D}(\mathbf{u}^h)$ are given by the tensor $\mathbb{G}^H$ which represents the L^2-projection of $\mathbb{D}(\mathbf{u}^h)$ into L^H and, consequently, the resolved small scales are given by $\mathbb{D}(\mathbf{u}^h) - \mathbb{G}^H$. Therefore, the additional viscous term $(\nu_T(\mathbb{D}(\mathbf{u}^h) - \mathbb{G}^H),\ \mathbb{D}(\mathbf{v}^h))$, introduced by the projection-based VMS methods in the momentum equation, acts directly only on the resolved small scales.

The parameters of (6) are ν_T and L^H. Since the large scales have been defined by a projection into this space, L^H must be in some sense coarser than the finite element spaces considered for all resolved scales. This can be achieved by choosing L^H of lower order than $V^h \times Q^h$, on the same grid, provided that $V^h \times Q^h$ are of high enough order, see [36] for a discussion of this topic. As turbulent viscosity, the static Smagorinsky model $\nu_T = C_S\delta^2\|\mathbb{D}(\mathbf{u}^h)\|_F$ will be used.

Numerical studies [19,21,22,26] have shown that the choice of the large scale space L^H is crucial for the obtained results. Already in [22], it has been proven that for the efficiency of the projection-based FEVMS method, L^H must be a piecewise polynomial but across the mesh cells discontinuous finite element space. Recently, in [20], this method has been extended such that L^H can be chosen a posteriorly with allowing different polynomial degrees in different mesh cells K. The aim is to adjust the local influence of the turbulence model according to the local turbulent character of the flow by an appropriate scale separation.

The a posteriori choice of L^H has to be controlled. For this purpose, the local L^2-norm of the resolved small scales $\mathbb{D}(\mathbf{u}^h) - \mathbb{G}^H$ is used. In the numerical studies, the velocity finite element space will be P_2^{bubble}. Then, for K being a mesh cell of a triangulation $\mathcal{T}^h$, $L^H(K)$ is allowed to vary from the space consisting only of the zero tensor, denoted by $P_{00}(K)$, to $P_0(K)$, $P_1^{\mathrm{disc}}(K)$, and $P_2^{\mathrm{disc}}(K)$ (the index disc indicates the discontinuity across the mesh cells). Thus, the local effect of the turbulence model varies from being locally applied to all resolved scales, for a strong turbulent character ($P_{00}(K)$), to (almost) being switched off ($P_2^{\mathrm{disc}}(K)$) for flow regions more or less laminar. In order to allow the possibility of switching off the turbulence model, we even set $\nu_T = 0$ for subregions with very little turbulence.

The adaptive FEVMS considers the size of the resolved small scales

$$\eta_K = \frac{\|\mathbb{D}(\mathbf{u}^h) - \mathbb{G}^H\|_{L^2(K)}}{\|1\|_{L^2(K)}} = \frac{\|\mathbb{D}(\mathbf{u}^h) - \mathbb{G}^H\|_{L^2(K)}}{|K|^{1/2}}, \quad K \in \mathcal{T}^h, \tag{7}$$

as local indicator of the amount of turbulence. The assumption behind this indicator is the expectation that in regions with high turbulence, where the size of the unresolved scales is large, also the size of the adjacent class of scales (the small resolved scales) is large. These indicators have to be compared with a reference value. The numerical studies presented below will use the arithmetic mean $\overline{\eta}$ of the local indicators. This choice has been proven reasonable in [20]. The local space $L^H(K)$ will be determined as follows: choose $0 \le C_1 \le C_2 \le C_3$, define $\eta := \eta_K/\overline{\eta}$, then

1. for cells K with $\eta \le C_1$: $L^H(K) = P_2^{\mathrm{disc}}(K)$, $\nu_T(K) = 0$,
2. for cells K with $C_1 < \eta \le C_2$: $L^H(K) = P_1^{\mathrm{disc}}(K)$,
3. for cells K with $C_2 < \eta \le C_3$: $L^H(K) = P_0(K)$,
4. for cells K with $C_3 < \eta$: $L^H(K) = P_{00}(K)$.

Compared with the projection-based FEVMS method with static large scale space L^H, the computation of G^H and η_K is an additional work. In addition, more matrices have to be updated during the simulation if the space L^H is changing. In the simulations presented below, the space L^H will be updated at each discrete time.

3. Numerical studies

3.1. The discretization of the models

The Crank–Nicolson scheme with an equidistant time step Δt was used for the temporal discretizations of the equations. This is an efficient and accurate scheme for equations modeling incompressible flows [37]. The discretization in space was

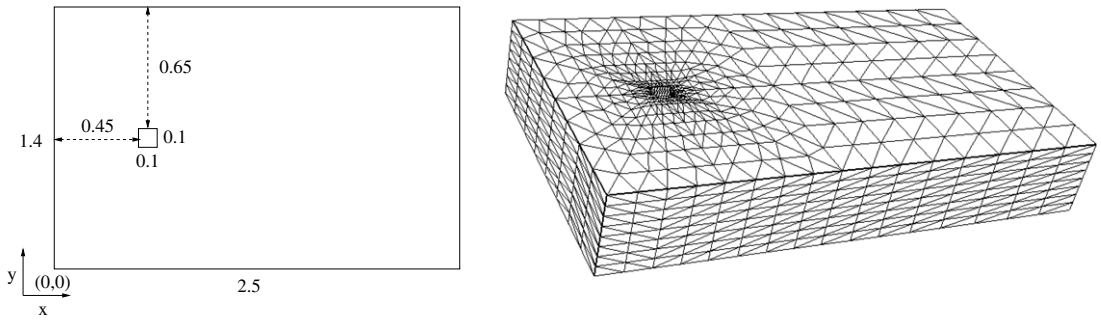

Fig. 1. Turbulent flow around a cylinder with square cross-section. Left: the cross-section of the domain (all lengths in m), the height of the channel is $H = 0.4$ m; right: tetrahedral grid used for the simulations.

performed with the $P_2^{\text{bubble}}/P_1^{\text{disc}}$ pair of finite elements, see [30]. Discontinuous pressure approximations lead to weakly divergence-free velocity fields on each mesh cell. In addition, coupled multigrid solvers turn out to work efficiently for discontinuous pressure approximations [28,29,38]. The nonlinearities of the equations were solved by a fixed point iteration.

For evaluating the last term on the left hand side in the rational LES model (5), an auxiliary problem equipped with homogeneous Neumann boundary conditions was solved, see [11] for details. For the FEVMS method, the fully implicit approach from [22] was used, see also [20]. All numerical simulations were performed with the code MooNMD [39].

3.2. The turbulent flow around a cylinder

The benchmark problem of a turbulent flow around a cylinder with squared cross-section at $Re = 20\,000$ was defined in [40]. The flow domain is presented in Fig. 1. The inflow is prescribed by $\mathbf{u}(t, 0, y, z) = (1 + 0.04\,\texttt{rand}, 0, 0)^{\mathrm{T}}$, with rand being a random number in $[-0.5, 0.5]$, the noise serving to stimulate the turbulence. At the column, no-slip boundary conditions were prescribed, whereas outflow boundary conditions were set at $x = 2.5$ and free slip condition on all other boundaries. The Reynolds number of the flow $Re = 22\,000$ is based on the mean inflow $U_\infty = 1$ m/s, the edge size of the cylinder $D = 0.1$ m and the viscosity $\nu = 1/220\,000$. It is assumed that no external forces act on the flow.

The computations were performed with 211 440 velocity degrees of freedom and 61 440 pressure degrees of freedom. Since the flow is strongly underresolved, the use of a turbulence model becomes necessary. In all turbulence models, we used as eddy viscosity the static Smagorinsky model with $\delta = 2\tilde{h}_K$, $\tilde{h}_K := |K|^{1/3}$ and $|K|$ being the volume of a mesh cell K. The time step was $\Delta t = 0.005$.

This example describes a statistically periodic flow. Functionals of interest are the drag c_d and the lift coefficient c_l at the cylinder and the Strouhal number St. For a detailed description of the computation of these values, we refer to [22,28]. For drag and lift, time-averaged values $\bar{c}_l$, $\bar{c}_d$ are given together with the corresponding rms values, which describe the mean amplitude of the oscillations around the time-averaged values. All computations were started with a fully developed flow field. They had 20 s to develop with respect to the used turbulence model and the temporal mean values were computed from the following 25 periods. A period starts with the lift coefficient changing from a negative to a positive value. Representative results are presented in Table 1. For the constants in the choice of the adaptive large scales, the same values found to be appropriate in [20] were considered.

The results show that $c_{l,\text{rms}}$ was predicted by all simulations within the experimental interval. The time-averaged drag $\bar{c}_d$ was overpredicted in all cases. Only the rational LES model was able to predict the corresponding rms value within the experimental range. However, one of these simulations showed a considerably larger error in the Strouhal number in comparison with all other simulations. It can be clearly seen that the VMS method with adaptive large scale space improved the results compared with the static uniform choice of this space. Firstly, we never observed a blow up in the adaptive VMS method and secondly, the time-averaged drag is clearly closer to the experimental value than for the VMS method with piecewise constant tensors.

3.3. The flow through a reactor with a torispherical head

This example considers a type of reactor geometry which is used in chemical engineering. For this geometry, we were not able to manually construct a hexahedral grid and we had no access to a hexahedral grid generator. Thus, a tetrahedral grid generated with TETGEN [41] was used in the simulations. Since there are no benchmark simulations available for flows through this kind of reactor, we will only show that the indicator (7) of the local turbulence intensities returns correct answers.

The geometry of the reactor is sketched in Fig. 2. It is a standard configuration flat flange cylindrical vessel of diameter D_1 with a torispherical head (defined as by DIN 28011 standards) and a flat closed surface. These kinds of heads have a dish with a fixed radius f_D, whose size depends on the type of torispherical head. The transition between the cylinder and the dish is made by a toroidal shape. The dish has a radius that equals the diameter of the cylinder it is attached to, $f_D = D_1$. The

Table 1
Turbulent flow around a cylinder with square cross-section. Time-averaged coefficients and rms values. In the VMS method with adaptive large scale space, $C_S = 0.01$ has been used.

	C_1	C_2	C_3	$\bar{c}_l$	$c_{l,\mathrm{rms}}$	$\bar{c}_d$	$c_{d,\mathrm{rms}}$	St
Smagorinsky LES ($C_S = 0.005$)				−0.053	1.30	2.58	0.099	0.138
Smagorinsky LES ($C_S = 0.0075$)				−0.033	1.20	2.50	0.082	0.137
Smagorinsky LES ($C_S = 0.01$)				−0.026	1.10	2.43	0.072	0.137
rational LES ($C_S = 0.005$)				0.092	1.13	2.33	0.136	0.144
rational LES ($C_S = 0.0075$)				0.012	1.38	2.51	0.128	0.139
FEVMS, $L^H = P_0$ ($C_S = 0.005$)				−0.098	1.22	2.61	0.076	0.139
FEVMS, $L^H = P_0$ ($C_S = 0.0075$)				−0.102	1.28	2.61	0.086	0.138
FEVMS, $L^H = P_0$ ($C_S = 0.01$)				−0.093	1.22	2.59	0.082	0.138
FEVMS, $L^H = P_1^{\mathrm{disc}}$				Blow up of the solver				
adap. FEVMS	0.2	0.7	2	−0.041	1.02	2.40	0.061	0.138
adap. FEVMS	0.2	0.8	2	−0.036	1.08	2.42	0.073	0.138
adap. FEVMS	0.2	0.7	3	−0.037	1.12	2.48	0.076	0.139
adap. FEVMS	0.2	0.8	3	−0.030	1.17	2.50	0.086	0.138
adap. FEVMS	0.3	0.7	2	−0.034	0.99	2.40	0.060	0.137
adap. FEVMS	0.3	0.8	2	−0.039	1.04	2.42	0.068	0.138
adap. FEVMS	0.3	0.7	3	−0.055	1.12	2.49	0.077	0.139
adap. FEVMS	0.3	0.8	3	−0.050	1.08	2.47	0.068	0.139
	Experiments				0.7–1.4	1.9–2.1	0.1–0.2	0.132

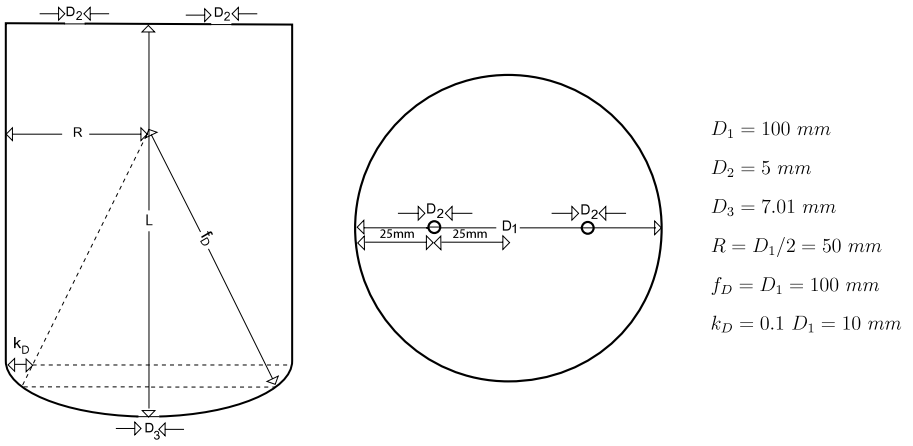

Fig. 2. Reactor with torispherical head, cut and top view. The total height of the reactor is $L = 140$ mm.

toroidal shape has a radius that equals a tenth of the diameter of the cylinder, $k_D = 0.1\ D_1$. There are two comparatively small inlets on the top of the reactor, which are located symmetrically with respect to the axis of the cylindrical reactor, each inlet having a diameter D_2. The outlet is placed in the middle of the spherical bottom and has the diameter D_3.

We considered the flow of water (kinematic viscosity $\nu = 10^{-6}$ m^2/s) with the inflow velocity $(0, 0, -U_\infty)$, $U_\infty = 0.1$ m/s. This leads, using as characteristic length scale $L_\infty = 10^{-3}$ m, to a Reynolds number of $Re = L_\infty U_\infty/\nu = 10^2$. Outflow boundary conditions are prescribed at the outlet. The computations were performed with the projection-based FEVMS method with $L^H(K) = P_0(K)$ for all mesh cells and $C_S = 0.01$ in the turbulent viscosity. The Crank–Nicolson scheme was applied with $\Delta t = 0.01$ and the $P_2^{\mathrm{bubble}}/P_1^{\mathrm{disc}}$ discretization had 139 887 degrees of freedom for the velocity and 39 680 degrees of freedom for the pressure. The grid is presented in (Fig. 3).

A high turbulence can be expected first at the inlets. There, the situation is similar to a backward facing step, and recirculation appears. A second subdomain with high turbulence will be in the torispherical head. The jets from the inlets will reach the head, they will be directed to the outlet and they will merge. In contrast, relatively low turbulence can be expected in the cylindrical vessel away from the jets. Fig. 4 shows that all expectations are correctly met by the indicator.

4. Summary

The paper studied several turbulence models on tetrahedral meshes. In particular, it was shown that a FEVMS method with an adaptive large scale space can be extended in a straightforward way to such meshes. Computations were performed with the $P_2^{\mathrm{bubble}}/P_1^{\mathrm{disc}}$ pair of finite element spaces. One could not distinguish one method to be better than all other ones. Only the adaptive VMS method gave improved results in comparison with the VMS method with uniform static large scale space. In addition, it was shown at a flow through a reactor that the indicator of the adaptive VMS method predicts the distribution of the turbulence intensities correctly.

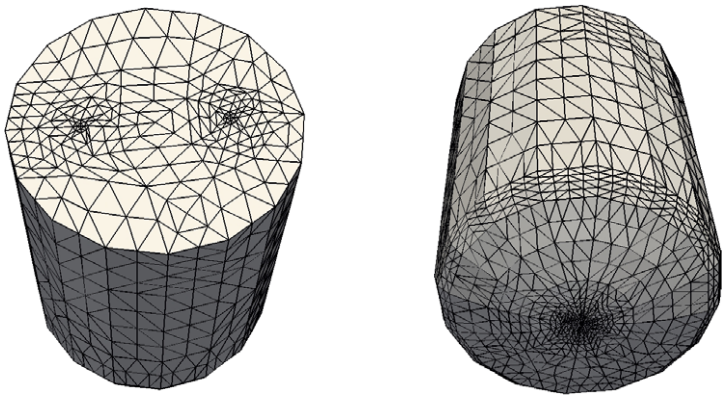

Fig. 3. Tetrahedral grid for the flow through a reactor.

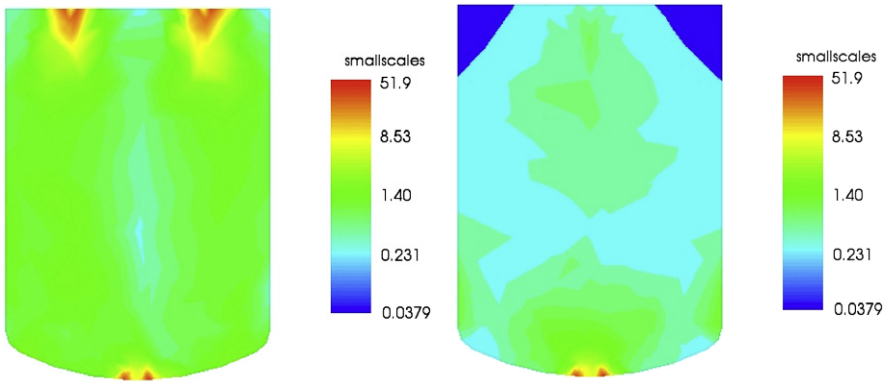

Fig. 4. Magnitude of the resolved small scales in the flow through the reactor, left: Cut plane $y = 0$ (containing the inlets), right: Cut plane $x = 0$.

Acknowledgements

The research of A. Kindl was supported by the Deutsche Forschungsgemeinschaft (DFG), grants No. Jo 329/7–1 and No. Jo 329/7–2. The research of C. Suciu was supported by the Bundesministerium für Bildung und Forschung (BMBF), grant 03JOPAA5.

References

[1] P. Sagaut, Large Eddy Simulation for Incompressible Flows, 3rd ed., Springer-Verlag, Berlin, Heidelberg New York, 2006.
[2] T.J.R. Hughes, Multiscale phenomena: Green's functions, the Dirichlet-to-Neumann formulation, subgrid-scale models, bubbles and the origin of stabilized methods, Comput. Methods Appl. Mech. Engrg. 127 (1995) 387–401.
[3] J.-L. Guermond, Stabilization of Galerkin approximations of transport equations by subgrid modeling, M2AN 33 (1999) 1293–1316.
[4] T.J. Hughes, L. Mazzei, K.E. Jansen, Large Eddy simulation and the variational multiscale method, Comput. Visual. Sci. 3 (2000) 47–59.
[5] J.S. Smagorinsky, General circulation experiments with the primitive equations, Mon. Weather Rev. 91 (1963) 99–164.
[6] M. Germano, U. Piomelli, P. Moin, W. Cabot, A dynamic subgrid-scale Eddy viscosity model, Phys. Fluids A 3 (1991) 1760–1765.
[7] D.K. Lilly, A proposed modification of the Germano subgrid-scale closure method, Phys. Fluids A 4 (1992) 633–635.
[8] A. Leonard, Energy cascade in large Eddy simulation of turbulent fluid flows, Adv. Geophys. 18A (1974) 237–248.
[9] G.P. Galdi, W.J. Layton, Approximation of the larger eddies in fluid motion II: A model for space filtered flow, Math. Models Methods Appl. Sci. 10 (3) (2000) 343–350.
[10] V. John, Large Eddy Simulation of Turbulent Incompressible Flows. Analytical and Numerical Results for a Class of LES Models, in: Lecture Notes in Computational Science and Engineering, vol. 34, Springer-Verlag, Berlin, Heidelberg, New York, 2004.
[11] V. John, An assessment of two models for the subgrid scale tensor in the rational LES model, J. Comp. Appl. Math. 173 (2005) 57–80.
[12] T. Iliescu, V. John, W.J. Layton, G. Matthies, L. Tobiska, A numerical study of a class of LES models, Int. J. Comput. Fluid Dyn. 17 (2003) 75–85.
[13] A. Dunca, V. John, W.J. Layton, The commutation error of the space averaged Navier–Stokes equations on a bounded domain, in: J.G. Heywood, G.P. Galdi, R. Rannacher (Eds.), Contributions to Current Challenges in Mathematical Fluid Mechanics, Birkhäuser, 2004, pp. 53–78.
[14] L.C. Berselli, V. John, Asymptotic behavior of commutation errors and the divergence of the Reynolds stress tensor near the wall in the turbulent channel flow, Math. Meth. Appl. Sci. 29 (2006) 1709–1719.
[15] L.C. Berselli, C.R. Grisanti, V. John, Analysis of commutation errors for functions with low regularity, J. Comput. Appl. Math. 206 (2007) 1027–1045.
[16] V. John, A. Liakos, Time-dependent flow across a step: The slip with friction boundary condition, Internat. J. Numer. Methods Fluids 50 (2006) 713–731.
[17] T.J.R. Hughes, G. Scovazzi, L.P. Franca, Multiscale and stabilized methods, in: E. Stein, R. de Borst, T.J.R. Hughes (Eds.), Encyclopedia of Computational Mechanics, John Wiley & Sons, 2004.
[18] V. John, On large Eddy simulation and variational multiscale methods in the numerical simulation of turbulent incompressible flows, Appl. Math. 51 (2006) 321–353.

[19] V. John, M. Roland, Simulations of the turbulent channel flow at $Re_\tau = 180$ with projection-based finite element variational multiscale methods, Internat. J. Numer. Methods Fluids 55 (2007) 407–429.
[20] V. John, A. Kindl, A variational multiscale method for turbulent flow simulation with adaptive large scale space. Universität des Saarlandes, Fachrichtung Mathematik, Preprint 228, 2009.
[21] V. John, A. Kindl, Numerical studies of finite element variational methods for turbulent flow simulations. Comput. Methods Appl. Mech. Engrg., 2009 (in press).
[22] V. John, S. Kaya, A finite element variational multiscale method for the Navier–Stokes equations, SIAM J. Sci. Comput. 26 (2005) 1485–1503.
[23] T.J.R. Hughes, L. Mazzei, A.A. Oberai, A.A. Wray, The multiscale formulation of large Eddy simulation: Decay of homogeneous isotropic turbulence, Phys. Fluids 13 (2001) 505–512.
[24] T.J.R. Hughes, A.A. Oberai, L. Mazzei, Large Eddy simulation of turbulent channel flows by the variational multiscale method, Phys. Fluids 13 (2001) 1784–1799.
[25] V. Gravemeier, Scale-separating operators for variational multiscale large Eddy simulation of turbulent flows, J. Comput. Phys. 212 (2006) 400–435.
[26] V. John, A. Kindl, Variants of projection-based finite element variational multiscale methods for the simulation of turbulent flows, Internat. J. Numer. Methods Fluids 56 (2008) 1321–1328.
[27] S. Ramakrishnan, S.S. Collis, Turbulence control simulation using the variational multiscale method, AIAA J. 42 (2004) 745–753.
[28] V. John, G. Matthies, Higher order finite element discretizations in a benchmark problem for incompressible flows, Internat. J. Numer. Methods Fluids 37 (2001) 885–903.
[29] V. John, On the efficiency of linearization schemes and coupled multigrid methods in the simulation of a 3d flow around a cylinder, Internat. J. Numer. Methods Fluids 50 (2006) 845–862.
[30] C. Bernardi, G. Raugel, Analysis of some finite elements for the Stokes problem, Math. Comput. 44 (1985) 71–79.
[31] S.B. Pope, Turbulent Flows, Cambridge University Press, 2000.
[32] J. Meyers, P. Sagaut, On the model coefficients for the standard and the variational multi-scale smagorinsky model, J. Fluid Mech. 569 (2006) 287–319.
[33] O.A. Ladyzhenskaya, New equations for the description of motion of viscous incompressible fluids and solvability in the large of boundary value problems for them, Proc. Steklov Inst. Math. 102 (1967) 95–118.
[34] A. Świerczewska, A dynamical approach to large Eddy simulation of turbulent flows: Existence of weak solutions, Math. Methods Appl. Sci. 29 (2006) 99–121.
[35] V. John, W.J. Layton, Analysis of numerical errors in large Eddy simulation, SIAM J. Numer. Anal. 40 (2002) 995–1020.
[36] V. John, S. Kaya, W. Layton, A two-level variational multiscale method for convection-dominated convection–diffusion equations, Comput. Methods Appl. Math. Engrg. 195 (2006) 4594–4603.
[37] V. John, G. Matthies, J. Rang, A comparison of time-discretization/linearization approaches for the time-dependent incompressible Navier–Stokes equations, Comput. Methods Appl. Mech. Engrg. 195 (2006) 5995–6010.
[38] V. John, Higher order finite element methods and multigrid solvers in a benchmark problem for the 3D Navier–Stokes equations, Internat. J. Numer. Methods Fluids 40 (2002) 775–798.
[39] V. John, G. Matthies, MooNMD — A program package based on mapped finite element methods, Comput. Visual. Sci. 6 (2004) 163–170.
[40] W. Rodi, J.H. Ferziger, M. Breuer, M. Pourquié, Status of large Eddy Simulation: Results of a workshop, J. Fluids Engrg. 119 (1997) 248–262.
[41] H. Si, Tetgen, A quality tetrahedral mesh generator and three-dimensional Delauny triangulator, v1.3 User's Manual. Technical Report 9, Weierstrass Institute Berlin, 2004.